Exploring topological edge states in photonic quasicrystals

F. Baboux*[1], E. Levy*[2,3], A. Lemaître[1], C. Gómez[1], E. Galopin[1],
L. Le Gratiet[1], I. Sagnes[1], A. Amo[1], J. Bloch[1,4], E. Akkermans[2]
*These authors contributed equally to this work.
[1]Centre de Nanosciences et de Nanotechnologies, CNRS, Univ. Paris-Sud,
Université Paris-Saclay, C2N Marcoussis, 91460 Marcoussis, France
[2]Department of Physics, Technion Israel Institute of Technology, Haifa 32000, Israel
[3]Rafael Ltd., P.O. Box 2250, Haifa 32100, Israel and
[4]Physics Department, Ecole Polytechnique, Université Paris-Saclay, F-91128 Palaiseau Cedex, France

(Dated: July 14, 2016)

We experimentally investigate the topological properties of quasiperiodic chains using cavity polaritons confined in a potential following the Fibonacci sequence. Edge states forming in the gaps of a fractal energy spectrum are imaged both in real and momentum space. These edge states periodically traverse the gaps when varying a structural degree of freedom ϕ of the Fibonacci sequence. The period and direction of the traverses are directly related to the Chern numbers assigned to each gap by the gap-labeling theorem. Additionally, we show that the Chern numbers determine the spatial symmetry properties of the edge states. These results highlight the potential of cavity polaritons to emulate nontrivial topological properties in a controlled environment.

PACS numbers: 03.65.Vf, 61.44.Br, 71.36.+c, 78.67.-n, 78.67.Pt

Topology has long been recognized as a powerful tool both in mathematics and in physics, where it generalizes the notion of symmetry class. It allows identifying families of structures which cannot be related by continuous deformations and are characterized by integer numbers called topological invariants. A physical example where topological features are particularly fascinating is provided by quantum anomalies in field theory, i.e. classical symmetries broken at the quantum level [1], such as the chiral anomaly recently observed in condensed matter [2]. From a general viewpoint, wave or quantum systems possessing a gapped energy spectrum, such as band insulators, superconductors, or 2D conductors in a magnetic field, can be assigned topological invariants called Chern numbers [3]. These Chern numbers control a variety of physical phenomena: for instance in the integer quantum Hall effect, they determine the value of the Hall conductance as a function of magnetic field [4, 5]. Such topological features related to Chern numbers have been explored in crystals [6] and more recently in various artificial periodic lattices for cold atoms [7–9], acoustic waves [10] or photons [11–16].

Quasicrystals – nonperiodic structures with long range order – [17, 18] are another important class of systems exhibiting topological effects [19–24], which have been recently investigated in photonic systems [22, 25–27]. A paradigmatic example of quasicrystal is given by the 1D Fibonacci chain. It presents a fractal energy spectrum made of an infinite number of gaps [28]. A hardly anticipated and fascinating property is that each of theses gaps can be assigned a Chern number: this constitutes the so-called gap-labeling theorem [29]. These Chern numbers q can take N integer values, N being the number of letters in the chain [30], and could potentially lead to the appearance of an infinite set of topological edge states in the gaps.

The physical origin of Chern numbers in the Fibonacci quasicrystal can also be related to its structural properties [31]. To understand this, let us introduce a general method - among others - to generate a Fibonacci sequence: it is based on the characteristic function

$$\chi_j = sign\left[\cos\left(2\pi\, j\, \sigma^{-1} + \phi\right) - \cos\left(\pi\, \sigma^{-1}\right)\right], \quad (1)$$

proposed in [32], which takes two possible values ± 1, respectively identified with two letters A and B representing e.g. two different values of a potential energy. A Fibonacci sequence of size N is a word $\vec{F}_N(\phi) \equiv [\chi_1\chi_2\cdots\chi_N]$ formed by A and B letters. In Eq. (1), $\sigma = (1+\sqrt{5})/2$ is the golden mean and ϕ is a parameter called phason, that can be continuously varied between 0 and 2π. The phason is a structural degree of freedom which allows selecting distinct finite segments along the infinite chain $\vec{F}_\infty$. Sweeping ϕ over a 2π–period induces a series of N independent local structural changes in the Fibonacci sequence $\vec{F}_N$. Each change corresponds to the inversion of two letters ($AB \leftrightarrow BA$) at a given location of the sequence (see vertical arrows in Fig. 1c). Importantly, for two particular values of ϕ within a period, the Fibonacci sequence $\vec{F}_N(\phi)$ becomes palindromic, i.e. it coincides with its mirror symmetric $\overleftarrow{F}_N(\phi) = [\chi_N\chi_{N-1}\cdots\chi_1]$. In between these two values, ϕ drives a 1D structural, π–periodic, symmetry cycle, and plays a role analogous to the magnetic field in the 2D quantum Hall effect. Interestingly enough, when concatenating $\vec{F}_N(\phi)$ with $\overleftarrow{F}_N(\phi)$, edge states appear at the interface whose properties are tightly linked to ϕ and to the Chern number q of the gap in which they appear [31].

In this Letter, we investigate the topological properties of Fibonacci quasicrystals using such edge states.

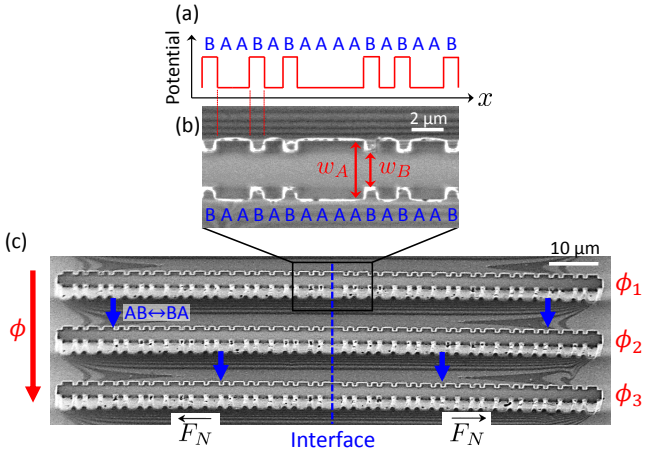

Figure 1. (a) Nominal potential energy corresponding to a laterally modulated 1D cavity. (b) Scanning electron microscopy (SEM) image of a portion of a 1D cavity reproducing the Fibonacci sequence (top view). The letters A and B correspond to two different widths of the cavity. (c) SEM image showing the full view of 3 fabricated Fibonacci structures, corresponding to 3 different values of the phason ϕ. Each structure consists of the concatenation $\overleftarrow{F}_N\overrightarrow{F}_N$ of a Fibonacci sequence $\overrightarrow{F}_N$ and its mirror symmetric $\overleftarrow{F}_N$. Vertical blue arrows indicate the position of local changes in the sequence introduced when scanning ϕ.

We employ cavity polaritons, quasiparticles arising from the strong coupling between excitons confined in quantum wells and photons confined in a semiconductor microcavity [33]. This photonic system allows emulating a variety of Hamiltonians [34–37] and characterizing the associated eigenstates both in the spectral and spatial domain [36]. Here, we harness these features to emulate topological edge states forming in the gaps of the fractal Fibonacci spectrum. Upon varying the phason ϕ, these edge states traverse the gaps, with a periodicity and direction along the energy axis directly determined by the gap Chern numbers. In addition to these spectral features, we show that additional information on the gap Chern numbers is also encoded in the spatial symmetry of the edge states, a robust feature largely insensitive to intrinsic disorder and other imperfections.

To explore the edge states, we design concatenated structures $\overleftarrow{F}_N\overrightarrow{F}_N$ made of the juxtaposition of a given Fibonacci sequence and its mirror symmetric (Fig. 1c). The interface defines a Fabry-Perot cavity of zero geometric length but finite round trip phase $\theta_{\rm cav}$ due to the reflexion between $\overrightarrow{F}_N$ and $\overleftarrow{F}_N$. Thus edge states will appear at energies $E_{\rm gap}(\phi)$, implicitly determined by the resonance condition $\theta_{\rm cav}(E_{\rm gap},\phi) = 2\pi m$, with $m \in \mathbb{Z}$. As detailed in [31], $\theta_{\rm cav}$ is periodic in ϕ with a period $\frac{\pi}{|q|}$, so that the evolution with ϕ of the edge states energy reflects directly the topological properties of the gap in which they appear.

To fabricate these structures, we process a planar microcavity (of nominal Q factor 70000) grown by molecular beam epitaxy. The cavity consists in a $\lambda/2$ $Ga_{0.05}Al_{0.95}As$ layer surrounded by two $Ga_{0.2}Al_{0.8}As/Ga_{0.05}Al_{0.95}As$ Bragg mirrors with 28 and 40 pairs in the top and bottom mirrors respectively. Twelve GaAs quantum wells of width 7 nm are inserted in the structure, resulting in a 15 meV Rabi splitting. Quasi-1D cavities (wires) are realized using electron beam lithography and dry etching. The lateral width of these wires is modulated quasi-periodically, as shown in the SEM image of Fig. 1b. The modulation consists in two wire sections A and B of same length $a = 1\,\mu$m, but different widths w_A and w_B. The width modulation induces an effective 1D potential for the longitudinal motion of polaritons (Fig. 1a), that follows the desired Fibonacci sequence. We chose $N = 55$ letters for the Fibonacci sequences and thus 110 letters for the concatenated structures. We have fabricated on a single sample the $N = 55$ concatenated structures corresponding to all values of ϕ producing a structural change in the sequence. Figure 1c shows a subset of three fabricated structures; the position of the interface between the mirror sequences $\overleftarrow{F}_N$ and $\overrightarrow{F}_N$ is indicated by a vertical line. The exciton-photon detuning is of the order of -20 meV for all experiments.

To study the polariton modes in these quasiperiodic structures, we perform low temperature (10 K) micro-photoluminescence experiments. Single structures are excited non-resonantly at low power, using a CW monomode laser at 740 nm. The excitation spot covers a $80\,\mu m$-long region centered on the interface. The emission is collected with a 0.5 numerical aperture objective and focused on the entrance slit of a spectrometer coupled to a CCD camera. Imaging the sample surface or the Fourier plane of the collection objective allows studying the polariton modes either in real or momentum space.

Figure 2 shows the real (a) and momentum space (b) photoluminescence of a Fibonacci structure with $\phi = 0.6\,\pi$, $w_A = 3.5\,\mu$m and $w_B = 2.2\,\mu$m. The energy spectrum shows an alternation of minibands and gaps. The emission in real space allows identifying two types of modes in the spectrum: modes delocalized over the whole structure, and modes (encircled) localized at the interface between the $\overleftarrow{F}_N$ and $\overrightarrow{F}_N$ sequences ($x = 0$). The delocalized modes form minibands, as can be seen in the momentum space emission: these modes are bulk modes forming a fractal energy spectrum characteristic of the Fibonacci quasicrystal, as previously evidenced in similar structures [38]. We can identify the main gaps of the spectrum by applying the gap-labeling theorem [29], which predicts $k = \frac{\pi}{a}(p+q\sigma^{-1})$ for the wavevector position of the gaps [39]. Here, p and q are integers, with q being the gap Chern number [29]. From the momentum space spectrum of Fig. 2b we extract $[p,q] = [-1,2]$ for

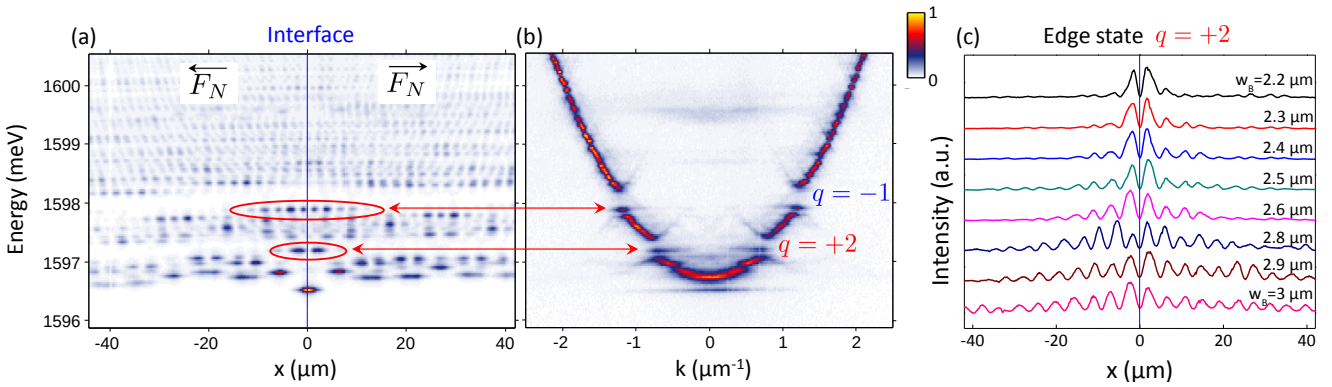

Figure 2. (a)-(b) Energy-resolved emission of a Fibonacci structure in real space (a) and in momentum space (b), for a given value of the phason ($\phi = 0.62\pi$). Edge states are visible in the two lowest energy gaps, characterized by $q = +2$ and $q = -1$. These states are localized at the interface ($x = 0$) between the $\overleftarrow{F}_N$ and $\overrightarrow{F}_N$ Fibonacci sequences. (c) Spatial profile of the edge state of gap $q = +2$ measured in a series of structures of same A-letter width $w_A = 3.5$ μm but various B-letter width w_B, yielding different contrasts for the Fibonacci potential.

the lower main energy gap, and $[p, q] = [1, -1]$ for the higher main energy gap.

In addition to the bulk states, we observe edge states localized at the interface between $\overrightarrow{F}_N$ and $\overleftarrow{F}_N$ and lying in the gaps of the fractal energy spectrum. Here, two such states are visible within the widest spectral gaps. Their spatial localization around the interface depends on the contrast of the Fibonacci quasiperiodic potential. Figure 2c shows the spatial profile (squared modulus of the wavefunction, $|\psi(x)|^2$) of the edge state of the gap $q = +2$, measured for a series of structures of same A-letter width $w_A = 3.5$ μm, but various B-letter widths w_B. As w_B decreases, the potential contrast (amplitude of the steps in Fig. 1b) increases: this leads to a steeper exponential decay of the edge state, and thus to a stronger spatial localization of the wavefunction.

To explore the topological properties of the Fibonacci sequences by means of these edge states, we will now monitor their evolution by varying the phason degree of freedom ϕ. We investigate a full set of $N = 55$ structures with $w_A = 3.5\,\mu$m and $w_B = 2.4\,\mu$m. For each structure, we perform spectroscopic measurements similar to Fig. 2a-b, and extract the energy of the two edge states with respect to the lowest bulk energy mode (bottom of the parabola, energy E_0). The results are plotted in Fig. 3a, where the gap boundaries are indicated by the horizontal lines. Numerical calculations based on a scattering matrix approach [31] are presented for comparison in Fig. 3c. Note that when $\phi = 0$ or π, no edge state is observed. Indeed, for these particular values of ϕ, the $\overrightarrow{F}_N$ sequence is palindromic and $\overleftarrow{F}_N\,\overrightarrow{F}_N$ effectively reduces to a single Fibonacci sequence of size $2N$. Hence there is no interface cavity and thus no edge state.

As clearly seen in Fig. 3a, while scanning the phason ϕ the states perform spectral traverses inside the gaps. The number and the direction of the traverses are given by the winding number [31]:

$$\mathcal{W} = \frac{1}{2\pi}\int_0^{2\pi} \frac{d\theta_{\rm cav}}{d\phi} d\phi = \frac{1}{2\pi}\int_0^{2\pi} \frac{d\widetilde{\delta}}{d\phi} d\phi = 2q \qquad (2)$$

where $\widetilde{\delta} \equiv \frac{E_{\rm gap} - E_-}{\Delta_g}$ is the spectral position of the edge state within the gap, with Δ_g being the gap width and E_- the energy of the gap lower boundary.

The direction and periodicity of the observed traverse is different for the two edge states we consider: the lower energy state traverses 4 times upwards (winding number $\mathcal{W} = +4$), while the higher energy state traverses 2 times downwards ($\mathcal{W} = -2$), when ϕ spans a full period $[0, 2\pi]$. This winding $\mathcal{W} = 2q$ of the edge states allows for a direct determination of the Chern numbers. We determine $q = +2$ for the lower energy state and $q = -1$ for the higher energy state. These values obtained from the winding of the *edge* states are fully consistent with those previously determined from the *bulk* band structure (gap-labeling theorem), illustrating the existence of a bulk-edge correspondence in this quasiperiodic system.

Finally, we investigate topological features in the spatial properties of the edge states. Figure 4 shows the measured profile of the $q = +2$ and $q = -1$ edge states for values of ϕ taken in the 4 successive quadrants: $[0, \pi/2]$, $[\pi/2, \pi]$, $[\pi, 3\pi/2]$ and $[3\pi/2, 2\pi]$. The states either show a maximum or a minimum intensity at the interface ($x = 0$), corresponding respectively to a symmetric (S) and anti-symmetric (AS) wavefunction. We observe that the $q = +2$ state (red) switches symmetry in each quadrant, while the $q = -1$ state (blue) keeps the same symmetry in the first two quadrants before switching to the opposite symmetry in the last two quadrants. The symmetry index (S or AS) is reported in Fig. 3b for all values of ϕ, and compared to theory in

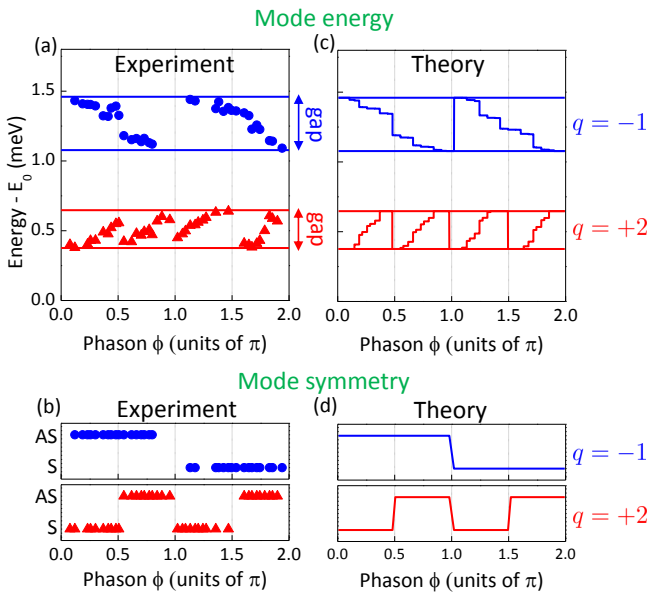

Figure 3. (a) Measured energy of the edge states of gaps $q = +2$ et $q = -1$ as a function of the phason ϕ. E_0 denotes the energy of the lowest bulk mode, and the solid lines indicate the gap boundaries. (b) Corresponding spatial symmetry of the edge states. When scanning ϕ, the wavefunctions evolve from symmetric (S) to anti-symmetric (AS) with respect to the interface ($x = 0$). (c) Relative spectral position within the gaps of the two considered edge states, obtained from scattering matrix calculations. (d) Calculated symmetry of the two considered edge states.

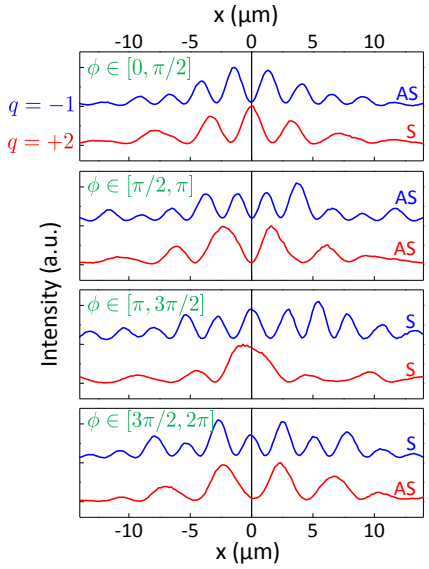

Figure 4. Measured spatial profile of the $q = +2$ and $q = -1$ edge states for values of ϕ taken in 4 different quadrants: $[0, \pi/2]$, $[\pi/2, \pi]$, $[\pi, 3\pi/2]$ and $[3\pi/2, 2\pi]$. The mode spatial structure switches from symmetric (S) to antisymmetric (AS) with respect to the interface ($x = 0$), with a direction and periodicity directly related to their Chern numbers.

Fig. 3d. Comparing this behavior to the spectral features reported in Fig. 3a-c, we observe that symmetry flips are exactly synchronized with the spectral traverse of the states: they occur in between two successive traverses. Their periodicity thus allows determining the absolute value of the Chern numbers. In addition, we observe that the sign of q is reflected in the direction of the symmetry flips within a period: the wavefunction of the $q = -1$ state switches from AS to S while that of the $q = +2$ state switches from S to AS. These features demonstrate that Chern numbers are not only encoded in the spectral properties of the edge states, but also in their spatial symmetry. This alternative access to the topology of quasicrystals could prove useful in other physical systems where the spectral degrees of freedom are less accessible.

In summary, we have investigated the topological properties of 1D Fibonacci photonic quasicrystals. We image edge states forming in the gaps of the fractal energy spectrum of the quasicrystals. The spectral and spatial behavior of these edge states upon varying a structural degree of freedom (phason) directly reflect the underlying topology of the system. This work demonstrates a novel approach to investigate the topological properties of quasicrystals. Taking advantage of the matter part of polaritons, it could be extended to probe the interplay of topology and interactions in quasicrystals [40] and potentially realize strongly correlated topological phases [41]. Furthermore, the building of cavities with topological mirrors could allow the investigation of the topological Casimir effect [42] in a well-controlled platform.

Acknowledgments: This work was supported by the Israel Science Foundation Grant No. 924/09, by the Agence Nationale de la Recherche project *Quandyde* (Grant No. ANR-11-BS10-001), the French *RENATECH* network, the European Research Council grant *Honeypol* and the EU-FET Proactive grant *AQuS* (Project No. 640800).

[1] D. J. Gross and R. Jackiw, Phys. Rev. D **6**, 477 (1972).
[2] J. Xiong, S. K. Kushwaha, T. Liang, J. W. Krizan, M. Hirschberger, W. Wang, R. Cava, and N. Ong, Science **350**, 413 (2015).
[3] S. S. Chern, *Complex Manifolds Without Potential Theory* (Springer-Verlag, New York-Heidelberg, 1979).
[4] K. v. Klitzing, G. Dorda, and M. Pepper, Phys. Rev. Lett. **45**, 494 (1980).
[5] J. Bellissard, A. van Elst, and H. Schulz-Baldes, Journal of Mathematical Physics **35**, 5373 (1994).
[6] M. Z. Hasan and C. L. Kane, Rev. Mod. Phys. **82**, 3045 (2010).
[7] N. Goldman, J. Dalibard, A. Dauphin, F. Gerbier,

M. Lewenstein, P. Zoller, and I. B. Spielman, Proceedings of the National Academy of Sciences **110**, 6736 (2013).
[8] M. Atala, M. Aidelsburger, J. T. Barreiro, D. Abanin, T. Kitagawa, E. Demler, and I. Bloch, Nature Physics **9**, 795 (2013).
[9] M. Aidelsburger, M. Lohse, C. Schweizer, M. Atala, J. T. Barreiro, S. Nascimbene, N. Cooper, I. Bloch, and N. Goldman, Nature Physics **11**, 162 (2015).
[10] M. Xiao, G. Ma, Z. Yang, P. Sheng, Z. Zhang, and C. T. Chan, Nature Physics **11**, 240 (2015).
[11] M. C. Rechtsman, J. M. Zeuner, Y. Plotnik, Y. Lumer, D. Podolsky, F. Dreisow, S. Nolte, M. Segev, and A. Szameit, Nature **496**, 196 (2013).
[12] M. Hafezi, Phys. Rev. Lett. **112**, 210405 (2014).
[13] W. Hu, J. C. Pillay, K. Wu, M. Pasek, P. P. Shum, and Y. D. Chong, Phys. Rev. X **5**, 011012 (2015).
[14] C. Poli, M. Bellec, U. Kuhl, F. Mortessagne, and H. Schomerus, Nature communications **6** (2015).
[15] S. A. Skirlo, L. Lu, Y. Igarashi, Q. Yan, J. Joannopoulos, and M. Soljačić, Phys. Rev. Lett. **115**, 253901 (2015).
[16] S. Mittal, S. Ganeshan, J. Fan, A. Vaezi, and M. Hafezi, Nature Photonics (2016).
[17] D. Shechtman, I. Blech, D. Gratias, and J. W. Cahn, Phys. Rev. Lett. **53**, 1951 (1984).
[18] D. Levine and P. J. Steinhardt, Phys. Rev. Lett. **53**, 2477 (1984).
[19] B. Simon, Advances in Applied Mathematics **3**, 463 (1982).
[20] H. Kunz, Phys. Rev. Lett. **57**, 1095 (1986).
[21] L.-J. Lang, X. Cai, and S. Chen, Phys. Rev. Lett. **108**, 220401 (2012).
[22] Y. E. Kraus, Y. Lahini, Z. Ringel, M. Verbin, and O. Zilberberg, Phys. Rev. Lett. **109**, 106402 (2012).
[23] Y. E. Kraus, Z. Ringel, and O. Zilberberg, Phys. Rev. Lett. **111**, 226401 (2013).
[24] S. Ganeshan, K. Sun, and S. Das Sarma, Phys. Rev. Lett. **110**, 180403 (2013).
[25] M. Verbin, O. Zilberberg, Y. E. Kraus, Y. Lahini, and Y. Silberberg, Phys. Rev. Lett. **110**, 076403 (2013).
[26] M. Verbin, O. Zilberberg, Y. Lahini, Y. E. Kraus, and Y. Silberberg, Phys. Rev. B **91**, 064201 (2015).
[27] P. Vignolo, M. Bellec, J. Böhm, A. Camara, J.-M. Gambaudo, U. Kuhl, and F. Mortessagne, Phys. Rev. B **93**, 075141 (2016).
[28] D. Damanik, M. Embree, A. Gorodetski, and S. Tcheremchantsev, Communications in Mathematical Physics **280**, 499 (2008).
[29] J. Bellissard, A. Bovier, and J.-M. Ghez, Reviews in Mathematical Physics **4**, 1 (1992).
[30] A. Dareau, E. Levy, M. Bosch Aguilera, R. Bouganne, E. Akkermans, F. Gerbier, and J. Beugnon, arXiv:1607.00901 (2016).
[31] E. Levy, A. Barak, A. Fisher, and E. Akkermans, arXiv:1509.04028 (2015).
[32] Y. E. Kraus and O. Zilberberg, Phys. Rev. Lett. **109**, 116404 (2012).
[33] C. Weisbuch, M. Nishioka, A. Ishikawa, and Y. Arakawa, Phys. Rev. Lett. **69**, 3314 (1992).
[34] M. Bayer, T. Gutbrod, A. Forchel, T. L. Reinecke, P. A. Knipp, R. Werner, and J. P. Reithmaier, Phys. Rev. Lett. **83**, 5374 (1999).
[35] N. Y. Kim, K. Kusudo, C. Wu, N. Masumoto, A. Löffler, S. Höfling, N. Kumada, L. Worschech, A. Forchel, and Y. Yamamoto, Nature Physics **7**, 681 (2011).
[36] I. Carusotto and C. Ciuti, Reviews of Modern Physics **85**, 299 (2013).
[37] F. Baboux, L. Ge, T. Jacqmin, M. Biondi, E. Galopin, A. Lemaître, L. Le Gratiet, I. Sagnes, S. Schmidt, H. E. Türeci, A. Amo, and J. Bloch, Phys. Rev. Lett. **116**, 066402 (2016).
[38] D. Tanese, E. Gurevich, F. Baboux, T. Jacqmin, A. Lemaître, E. Galopin, I. Sagnes, A. Amo, J. Bloch, and E. Akkermans, Phys. Rev. Lett. **112**, 146404 (2014).
[39] This property, exact in the limit of infinite chains, constitutes an excellent approximation for the considered structure length, as shown in Ref. [38].
[40] B. Freedman, G. Bartal, M. Segev, R. Lifshitz, D. N. Christodoulides, and J. W. Fleischer, Nature **440**, 1166 (2006).
[41] X.-G. Wen, Advances in Physics **44**, 405 (1995).
[42] M. Bordag, G. L. Klimchitskaya, U. Mohideen, and V. M. Mostepanenko, *Advances in the Casimir effect* (OUP Oxford, 2009).